Model approach for low-energy inelastic atomic collisions and application to Al + H and Al+ + H−

Andrey K. Belyaev[*]

Department of Theoretical Physics, Herzen University, Moika 48, St. Petersburg 191186, Russia;
Department of Physics and Astronomy, Uppsala University, S-75120 Uppsala, Sweden;
and Max-Planck-Institut für Astrophysik, D-85741 Garching bei München, Germany

A model approach is derived for estimates of cross sections and rate coefficients in low-energy inelastic collisions of hydrogen atoms and negative ions with other atoms and positive ions, which are of astrophysical interests. The approach is based on the asymptotic method for electronic molecular structure determination and on the branching probability current method for a nonadiabatic nuclear dynamical treatment. The derived approach is applied to low-energy Al + H and Al+ + H− inelastic collisions. It is shown that the processes with the largest values of cross sections and rates are the excitation and de-excitation ones between the Al($3d$) and Al($4p$) states in collisions with H, as well as the ion-pair formation and the mutual neutralization processes between these states and the ionic state; the second largest cross sections correspond to the similar processes involving the Al($4s$) state. The mechanisms of the processes are discussed in detail.
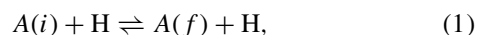
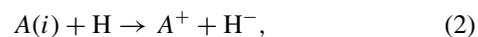PACS number(s): 34.10.+x, 34.50.Fa, 34.70.+e, 95.30.Dr

I. INTRODUCTION

Nonlocal thermodynamic equilibrium (non-LTE) effects are important for many fundamental problems in modern astrophysics; see, for example, [1–5], in particular, for stellar atmosphere modeling, for relative and absolute stellar chemical abundances, for the Galactic evolution, and so on. A non-LTE study requires detailed and complete information about the radiative and inelastic collision processes which affect the statistical equilibrium for a given atomic species. The most important inelastic collisions are ones with electrons and with hydrogen atoms and negative ions. The latter are a main source of uncertainty for non-LTE studies due to large concentrations of hydrogen atoms [1,2,5].

Recently, the progress has been achieved in detailed quantum treatments of inelastic processes in collisions of different atoms with hydrogen atoms. The accurate quantum cross sections were calculated for transitions between many low-lying atomic and ionic states for Na, Li, Mg + H collisions [6–10] based on accurate *ab initio* or pseudopotential quantum-chemical data [6,9,11–14]. The following processes in those collisions have been studied in details: the excitation and de-excitation,

$$A(i) + \mathrm{H} \rightleftharpoons A(f) + \mathrm{H}, \qquad (1)$$

the ion-pair formation,

$$A(i) + \mathrm{H} \rightarrow A^+ + \mathrm{H}^-, \qquad (2)$$

and the mutual neutralization processes

$$A^+ + \mathrm{H}^- \rightarrow A(f) + \mathrm{H}, \qquad (3)$$

A being an atom of interest, and i, f labeling electronic states of A. The quantum cross sections [6–10] were used for computing the inelastic rates [15–17] and finally for non-LTE astrophysical applications [15,18–20].

For many atoms of interest, however, quantum cross sections for inelastic collisions with hydrogen atoms are still not available. For this reason, the so-called "Drawin formula" [1,21], which is an extension [22] of a classical Thomson model, is still widely employed for estimates of inelastic cross sections for the processes (1)–(3). It has been shown in Ref. [23] (see also references therein) that for low-energy atomic collisions the Drawin formula does not have a correct physical background; it overestimates inelastic rates up to several orders of magnitude for optically allowed atomic transitions and underestimates rates for optically forbidden transitions. A use of scaling factors does not improve estimates obtained by means of the Drawin formula. First of all, fluctuations of scaling factors are huge: For example, for inelastic Mg + H collision rates a scaling factor was varied from 1 [24] until 0.001 [25] and even down to 3×10^{-10} [26]. What is more important is that the Drawin formula provides wrong relative efficiencies for different transitions: Even if a scaling factor is taken of a proper value for one transition, it does not give reliable rates for other transitions. Obviously, using the Drawin formula for low-energy inelastic atomic collisions is inappropriate and leads to unreliable results.

For this reason, Ref. [23] emphasized the importance of deriving an approximate model approach to inelastic atomic collisions with hydrogen atoms, an approach which would be physically reliable, but computationally not so expensive as a complete quantum study. This is the goal of the present paper. The model is demonstrated for the example of low-energy inelastic Al + H and Al+ + H− collisions. These collisions are of astrophysical interest [27–30]. For example, with the Gaia-ESO survey the Al abundance is measured for almost 100 000 stars. In addition, Al is an interesting element from the Galactic archeology perspective.

II. MODEL APPROACH

A. General remarks

The majority of theoretical treatments of inelastic collisions involving atoms, ions, molecules, etc., is performed within the standard adiabatic Born-Oppenheimer (BO) approach (or simply "the BO approach"), which is described, e.g.,

———————
[*]belyaev@herzen.spb.ru

in [31,32]. The approach is based on the separation of the electronic and nuclear motion. At first, the electronic fixed-nuclei Hamiltonian is treated and the electronic molecular states are determined, then the nuclear dynamics is studied. Thus, within the BO approach a collision problem is attacked in two steps: (i) evaluation of molecular potential energies and nonadiabatic couplings, and (ii) a study of the nonadiabatic nuclear dynamics. The proposed model is derived within the BO approach and based on these two steps. The model simplifies each of the steps in such a way as to avoid expensive calculations, but to keep physical reliability. The proposed model is derived at two levels. The simple model takes into account only nonadiabatic regions formed by long-range ionic-covalent interactions, while the extended model includes some additional nonadiabatic regions in order to estimate influence of these regions on transition probabilities, cross sections, and rates.

As described in Ref. [10], there are several mechanisms for inelastic processes (1)–(3). They correspond to two kinds of nonadiabatic regions: (i) long-range nonadiabatic regions due to ionic-covalent interactions, and (ii) (rather) short-range regions. The previous quantum studies [6–10] show that the largest values of inelastic cross sections are provided by nonadiabatic transitions at long-range regions. In the zero-order approximation, an inelastic cross section σ_{if} for a transition $i \rightarrow f$ can be roughly estimated by the following formula:

$$\sigma_{if} = p_i^{\text{stat}} \pi R_{\text{nonad}}^2 \bar{P}_{if}, \qquad (4)$$

where p_i^{stat} is a statistical probability for population of an initial channel i, R_{nonad} is the internuclear distance at which a center of a proper nonadiabatic region occurs, and $\bar{P}_{if}$ is a mean probability for this transition. In the simplest case, $\bar{P}_{if}$ is a mean transition probability in a nonadiabatic region in a vicinity of R_{nonad} after a double traverse of the region. Usually there are many nonadiabatic regions contributing in a final transition probability, so Eq. (4) should be treated as a rough upper-limit estimate for an inelastic cross section. As seen from Eq. (4), large cross sections correspond to large values of R_{nonad}, long-range nonadiabatic regions. On the other hand, at large internuclear distances R, transition probabilities $\bar{P}_{if}$ are small. This can be seen within the Landau-Zener (LZ) model [33] (see below). Finally, there is an optimal window of atomic states, for which inelastic cross sections have largest values, and this window corresponds to long-range nonadiabatic regions created by ionic-covalent interactions.

Thus, the developed model in its simple version is addressed to determination of long-range nonadiabatic regions with further calculations of cross sections and rate coefficients for inelastic processes with relatively large values. An extension of the simple model allows one to estimate how short-range nonadiabatic regions affect inelastic cross sections and rate coefficients.

B. Molecular potential energy curves

Ground-state potential energy curves (PECs) are known for many hydrides; see, e.g., Refs. [34,35]. They are important for rovibrational molecular structure, but not of much help for inelastic collisions. For a few hydrides, electronic structure calculations have been also performed for a couple of low-lying excited states, which allows one to compute excitation cross sections between ground and a few low-lying states. The number of complete sets of quantum-chemical data, including higher-lying and ionic states, is very limited [11,12,14]. So, one needs to evaluate PECs for many molecular states, including ionic, in order to estimate cross sections for the processes (1)–(3).

Within the proposed model, adiabatic molecular PECs for the processes of interest are calculated by diagonalizing the electronic (fixed-nuclei) Hamiltonian matrix at a grid of the internuclear distance R for molecular symmetries, which include ionic states. The basis set used consists of ionic ($A^+ + H^-$) and covalent ($A^* + H$) electronic wave functions. In its simplest version, only one ionic and several covalent states are taken into account though several ionic states can be treated as well. Diagonal elements of the Hamiltonian matrix H_{jj}, which represent diabatic potential energies, are taken as a sum of long-range and short-range potentials,

$$H_{jj}(R) = U_j^{\text{long}}(R) + U_j^{\text{short}}(R), \qquad (5)$$

j numbering a (diabatic) molecular state. Note that Eq. (5) is used for calculations of diabatic PECs at any R. Long-range potentials are constructed as a sum of their asymptotic values $U_j(\infty) = E_j^\infty$ (obtained from atomic and ionic energies) and potentials for long-range interactions V_j^{long}:

$$U_j^{\text{long}}(R) = E_j^\infty + V_j^{\text{long}}(R). \qquad (6)$$

For the ionic diabatic state, $A^+ + H^-$, V_j^{long} is determined by the screened Coulomb potential:

$$V_j^{\text{long}}(R) = -\frac{1 - \exp(-\tau R^2)}{R}, \qquad (7)$$

τ being a parameter of a molecular system, while for covalent states the long-range interactions are neglected. The short-range potentials are constructed from ones due to the exchange interaction and the screened nuclear repulsion,

$$U_j^{\text{short}}(R) = V_j^{\text{exch}}(R) + V^{\text{nucl}}(R). \qquad (8)$$

The exchange potentials are taken in the form [36],

$$V_j^{\text{exch}}(R) = A_j \exp(-\gamma_j R), \qquad (9)$$

where A_j and γ_j are parameters of the system; they are different for ionic and covalent states. The screened nuclear interaction potentials have the following form:

$$V^{\text{nucl}}(R) = \frac{Z_A}{R} \exp(-\tau R); \qquad (10)$$

they are the same for ionic and covalent states. Z_A is a nuclear charge of an atom A.

A semiempirical formula for one-electron charge exchange given in Ref. [37] is used in the present work for off-diagonal matrix elements H_{jk} ($j \neq k$) between an ionic and a covalent state. The formula yields

$$H_{jk}(R) = C_{jk} R \exp(-\alpha_{jk} R), \qquad (11)$$

where the parameters C_{jk} and α_{jk} are defined as

$$C_{jk} = \beta_{jk}\sqrt{I_{A^*(k)}\,I_{H^-}}, \tag{12}$$

$$\alpha_{jk} = 0.86\,\beta_{jk}, \tag{13}$$

while the parameter β_{jk} reads

$$\beta_{jk} = (\sqrt{I_{H^-}} + \sqrt{I_{A^*(k)}})/\sqrt{2}, \tag{14}$$

I_{H^-} and $I_{A^*(k)}$ being ionization potentials of corresponding orbitals in H^- and $A^*(k)$, respectively. The index j corresponds to an ionic diabatic molecular state $A^+ + H^-$, while the index k labels a covalent diabatic molecular state $A(k) + H$. This formula has been applied to a large number of one-electron transfer systems, including various mutual neutralization processes, and found to yield physically correct results [37]. Equation (11) provides a correct asymptotic behavior of off-diagonal matrix elements for charge exchange processes in agreement with the asymptotic theory; see, e.g., Ref. [38]. At short internuclear distances, Eq. (11) is expected to underestimate off-diagonal matrix elements. The off-diagonal matrix elements between covalent states are neglected in the present model approach.

Thus, the described procedure provides the Hamiltonian matrix in the arrow form (the only nonzero row, the only nonzero column, and the nonzero diagonal). Diagonalization of the so-obtained Hamiltonian matrix yields adiabatic molecular potential energies. It is worth pointing out that the formulas described above have several parameters, but the long-range matrix elements are determined by uniquely defined parameters (taken from atomic data), while short-range matrix elements depend on some parameters which do not come directly from atomic data. This leads to the fact that distant adiabatic PECs are well defined, while there is some freedom at short distances. Since the main interest is in calculations of long-range nonadiabatic regions created by the ionic-covalent configuration interaction, the described model approach is expected to determine these long-range potentials rather accurately and unambiguously. Some freedom at short distances allows one to adjust obtained adiabatic PECs to accurate *ab initio* calculations, which are available for ground and a few low-lying states in some cases, and this adjustment is expected not to affect nonadiabatic dynamics substantially. The particular application of this approach to the AlH molecule is described below.

The described approach was tested for a magnesium hydride for which the nine lowest *ab initio* adiabatic $^2\Sigma^+$ PECs have been calculated [9,10,14]. The long-range adiabatic PECs obtained by means of the model approach agree reasonably well with the accurate *ab initio* PECs. This is the result of the physically meaningful diabatic long-range PECs and reliable asymptotic off-diagonal matrix elements [Eqs. (11)–(14)], justified by various applications [37].

C. Nonadiabatic nuclear dynamics

In general, a known Hamiltonian matrix allows one to calculate not only adiabatic potentials, but also nonadiabatic couplings needed for quantum nuclear dynamical treatments. The present model approach is based on an approximate treatment of the nonadiabatic nuclear dynamics, which requires adiabatic potential curves only.

As is well known, hydride adiabatic PECs of a proper symmetry exhibit a series of avoided crossings at large internuclear distances formed by the ionic-covalent configuration interaction; see, for example, [7–12,14,34,35]. The model approach reported above clearly describes this kind of series. There is no simple general quantum solution for estimating a nonadiabatic transition probability P_{if} (for a transition $i \to f$) in case of several nonadiabatic regions, but using the Demkov-Osherov approach [39] one can approximately evaluate P_{if} via a sequence of single traverses of nonadiabatic regions with nonadiabatic transition probabilities p_{jk} in each region along different paths on the way in and out. Using this approximation, to account for several channels, the multichannel models have been proposed [40–42] in which nonadiabatic regions are passed in a particular order, that is, a single initial diabatic PEC crosses several noninteracting final diabatic PECs. These models are well suited for mutual neutralization processes (3), as well as for their inverse processes, the ion-pair formation ones (2), when all channels are open and there are no additional short-range transitions. The analytic formulas of Refs. [41,42] have been generalized in Ref. [7] for the excitation processes (1) also assuming that all channels are open. In particular, for the mutual neutralization processes, the probability P_{if}^F for a transition from an initial (ionic) state i to a final (covalent) state f in the presence of F final channels after a double passage of all nonadiabatic regions is written as a product of three factors:

$$P_{if}^F = P_i^{f-1}\,P_{if}\,P_{f+1}^F, \tag{15}$$

where P_i^{f-1} represents a probability for a system to survive in the initial diabatic state i after a traverse of first $f-1$ nonadiabatic regions; $P_{if} = 2p_{if}(1 - p_{if})$ is a probability of a transition $i \to f$ in a two-channel approximation, p_{if} being a transition probability after a single traverse of the nonadiabatic region created by the initial i and the final f diabatic states; P_{f+1}^F takes into account the presence of channels lying below channel f, that is, starting from $f+1$; see Refs. [41,42] for details. The advantage of Eq. (15) is that it gives the transition probability P_{if}^F in the analytic form, which simplifies calculations substantially, but the expression (15) is valid only for a particular order of nonadiabatic regions and only when all treated channels are energetically open, which is not always the case.

In practical applications, incoming and outgoing currents are distributed among many channels after traversing many nonadiabatic regions without any particular order. The approach which takes this into account has been recently proposed in Ref. [43], the so-called branching classical trajectory method: All nonadiabatic regions are accounted for by classical trajectories in any order that they appear during a collision. The basis of the method is twofold: branching of a classical trajectory and the novel formulas for LZ nonadiabatic transition probabilities adapted for classical trajectories [43].

The present model approach is based on the same ideas, but no classical trajectories are calculated. Instead of them, branching probability currents, both incoming and outgoing, are computed along effective adiabatic PECs as a function of

the internuclear distance R. A collision process is treated as a probability current evolution with varying R. A given collision energy E and a given total angular momentum quantum number J generate a unit incoming probability current in the initial channel at sufficiently large R (in an asymptotic region). The code runs over R downwards to classical turning points and then back upwards to an asymptotic region for each possible pathway. After each traverse of a nonadiabatic region, each probability current branches into two currents keeping the old path along the old adiabatic PEC and creating a new path along a new adiabatic PEC coupled in this nonadiabatic region with the old state; each of these currents is determined by the old current and the nonadiabatic transition probability in this nonadiabatic region. This approach is similar to the splitting of quantum probability currents taking place in rigorous quantum treatments of inelastic atomic collisions [6,36]. Thus, the code starts with a single incoming current and then generates new currents after traversing nonadiabatic regions according to all possible pathways. If a current for a new path is smaller than a critical value, a new current is not created; if a remaining current after passing a nonadiabatic region is smaller than the critical value, the old current is stopped, and the remaining current is transported into a new path. A final transition probability P_{if} is calculated as a sum of all outgoing probability currents for a final state f in the asymptotic region ($R \to \infty$) over all pathways created from an initial-channel incoming probability current by branching currents into all nonadiabatic regions in any order that they appear during a collision. The present approach can be called "the branching probability current method."

The important feature of the branching probability current method (as well as any surface-hopping approach) is a way of calculating nonadiabatic transition probabilities, which distinguishes different methods [44,45]. In the present branching probability current method, transition probabilities are calculated within the LZ model by the formula obtained in Ref. [43] that does not require a diabatization procedure; see below. Within the LZ model, the center of a nonadiabatic region corresponds to a minimum of an adiabatic splitting $Z_{jk} = |U_j - U_k|$, $U_{j,k}(R)$ being (effective) adiabatic potentials for states j and k. This fact is used for determination of nonadiabatic regions: The code calculates splitting Z_{jk} between adjacent adiabatic potentials as a function of R; if the function $Z_{jk}(R)$ attains a local minimum, this distance is taken as a center of a nonadiabatic region. The main assumption of the approach, the applicability of LZ estimates, is valid when there is physical evidence for avoided crossings, such as ionic-covalent crossings or a clear structure of adiabatic potentials. Obviously, the LZ model does not cover the whole variety of nonadiabatic effects, as stated in Ref. [44]: As with any mixed quantal-classical dynamics approach, a method cannot succeed in all situations, e.g., in cases of quantum interference. Nevertheless, in the present case, the method is expected to provide reliable estimates: There are avoided-crossing evidences and the LZ model works better for narrow nonadiabatic regions which provide large inelastic cross sections, which are, in turn, of the main interest in astrophysical applications. In addition, the proposed method allows one to calculate incoming and outgoing currents and to determine a mechanism of a process.

As mentioned above, the way of incorporating nonadiabatic transitions is crucial. Since the LZ model [33] is the most applicable one, it is used in the present approach. Within this two-state model, the probability p_{if}^{LZ} for the nonadiabatic transition $i \to f$ after a single traverse of a nonadiabatic region is expressed by the conventional analytical formula,

$$p_{if}^{\mathrm{LZ}} = \exp\left(-\frac{\xi_{if}}{v}\right), \qquad (16)$$

ξ_{if} being a parameter of the LZ model. In a diabatic representation it is defined as follows:

$$\xi_{if} = \frac{2\pi H_{if}^2}{\hbar |H_{ii}' - H_{ff}'|}. \qquad (17)$$

H_{if} is a constant off-diagonal matrix element, H_{ii} and H_{ff} are linear R-dependent diagonal matrix elements, v is a radial velocity of colliding atoms, which can be expressed in terms of a collision energy E and a total angular momentum quantum number J,

$$v = \sqrt{\frac{2}{\mu}\left(E_{\mathrm{total}} - U_c - \frac{J(J+1)\hbar^2}{2\mu R^2}\right)}, \qquad (18)$$

μ being the reduced mass of colliding particles, and $E_{\mathrm{total}} = E + U_i(\infty)$ being a total energy. All values are evaluated at the center of the nonadiabatic region R_c, where diabatic potentials cross $H_{ii}(R_c) = H_{ff}(R_c) = U_c$. Primed quantities are referred to derivatives with respect to the internuclear distance R.

Although Eq. (17) looks straightforward for computing an LZ parameter ξ_{if} in a particular nonadiabatic region of interest, there are some difficulties in its practical applications. First of all, in many cases quantum-chemical data are known in an adiabatic representation, moreover, only adiabatic PECs are known, but not nonadiabatic couplings. Since diabatic states are not uniquely defined, there is some ambiguity in calculations of diabatic matrix elements required in Eq. (17) from adiabatic PECs. Secondly, if quantum-chemical data are given in a diabatic representation, they are usually multichannel, while the LZ model is formulated in a two-state diabatic representation. As is well known (see, e.g., Ref. [8]), diabatic PECs and off-diagonal matrix elements in a multistate diabatic representation may deviate substantially from those in a two-state diabatic representation, and an additional transformation is required from a multistate diabatic representation to a two-state one. The novel procedure derived in Ref. [43] for calculations of LZ parameters from adiabatic PECs is free from these problems. The procedure is the following.

A diabatic representation allows one to calculate adiabatic potentials $U_i(R)$ and $U_f(R)$, as well as the splitting $Z_{if}(R)$. In a two-state case, it can be done analytically,

$$Z_{if}(R) = \sqrt{(H_{ii} - H_{ff})^2 + 4H_{if}^2}. \qquad (19)$$

Within the LZ model, this leads to

$$H_{if} = Z_{if}(R_c)/2, \qquad (20)$$

and, hence, to a relation between $|H_{ii} - H_{ff}|$ and $Z_{if}(R)$,

$$|H_{ii} - H_{ff}| = \sqrt{Z_{if}^2(R) - Z_{if}^2(R_c)}, \qquad (21)$$

which gives a slope difference derived via the splitting,

$$|H'_{ii} - H'_{ff}| = \sqrt{Z_{if} Z''_{if}} \tag{22}$$

at R_c. It turns out that the LZ parameter is written by means of the following formula:

$$\xi_{if} = \frac{\pi}{2\hbar} \sqrt{\frac{Z^3_{if}}{Z''_{if}}} \Bigg|_{R=R_c}, \tag{23}$$

which expresses the LZ parameter only in terms of the adiabatic splitting Z_{if} and its second distance derivative at R_c. Finally, within the LZ model the nonadiabatic transition probability is given by Eq. (16) with the parameter ξ_{if} written in the form (23). Equations (16) and (23) can be called the adiabatic-potential-based transition probability formulas.

Having transition probabilities known, inelastic cross sections are calculated as a sum over a total angular momentum quantum number J,

$$\sigma_{if}(E) = \frac{\pi \hbar^2 p_i^{\text{stat}}}{2 \mu E} \sum_{J=0}^{\infty} P_{if}(J,E)(2J+1). \tag{24}$$

Rate coefficients $K_{if}(T) = \langle \sigma_{if} v \rangle$ are then obtained by integrating over a collision energy E assuming the Maxwellian distribution valid,

$$K_{if}(T) = \sqrt{\frac{8}{\pi \mu (k_B T)^3}} \int_0^{\infty} \sigma_{if}(E) E \exp\left(-\frac{E}{k_B T}\right) dE, \tag{25}$$

T being a temperature, and k_B the Boltzmann constant.

The similar approach, the branching classical trajectory method, has been derived in Ref. [43] and applied to nonadiabatic nuclear dynamics in inelastic low-energy Na + H collisions. It was verified [43] that the method provides good agreement with complete quantum calculations [8], except for quantum interference (see also comparison in Fig. 1 for the ion-pair formation processes in Na(4s, 3d) + H collisions). The difference between the branching classical trajectory method [43] and the present branching probability current method is the following. Within the framework of the branching classical trajectory method, nonadiabatic transition probabilities are calculated via adiabatic splittings (and its second time derivative) as a function of time along classical trajectories by means of the following formula [43]:

$$p_{if} = \exp\left(-\frac{\pi}{2\hbar} \sqrt{\frac{Z^3_{if}}{\ddot{Z}_{if}}}\right). \tag{26}$$

In the present method the LZ parameters and the probabilities are calculated via splittings as a function of the internuclear distance [Eqs. (16) and (23)], that is, by means of varying R without calculating any classical trajectories. Equation (26) has an advantage in multidimensional cases, when a system passes the same nonadiabatic region along different trajectories and with different potential-energy profiles. In one-dimensional cases, a profile is the same for different trajectories, so within the present method the LZ parameters can be calculated only once by means of Eq. (23) and then
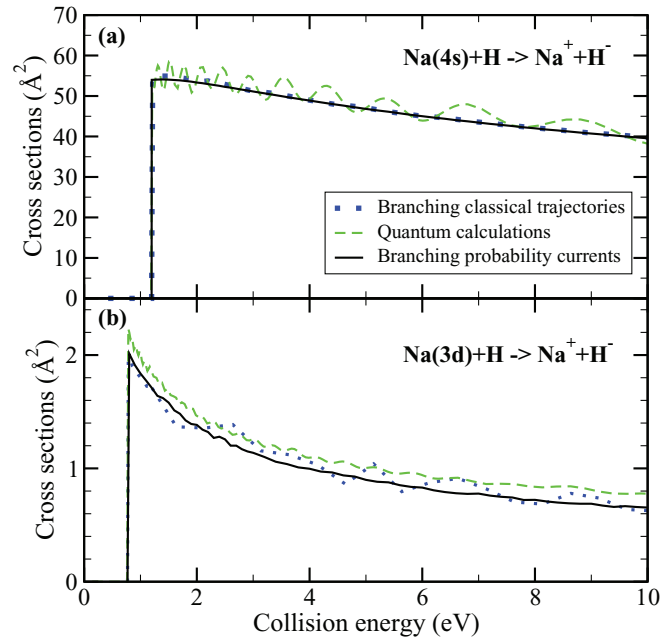

FIG. 1. (Color online) Comparison of cross sections for the ion-pair formation processes calculated by different methods: (a) Na(4s) + H → Na$^+$ + H$^-$; (b) Na(3d) + H → Na$^+$ + H$^-$. Dashed (green) lines, quantum calculations [8]; dotted (blue) lines, the branching classical trajectory method; solid (black) lines, the branching probability current method.

used for all dynamical calculations (with different J and E). This simplifies a nonadiabatic nuclear dynamical study and increases an accuracy. The comparison of the branching probability current method with the branching classical trajectory method and the complete quantum calculations is shown in Fig. 1 for the ion-pair formation processes with the largest cross sections in Na* + H collisions. It is seen that when the main nonadiabatic region for a given process is rather broad, Na(4s) + H collisions, the agreement of two branching methods is perfect. When the main nonadiabatic region is rather narrow, Na(3d) + H collisions, the branching classical trajectory method exhibits some dispersion related to a finite time step for classical trajectories, while the branching probability current method provides smooth cross sections. Decreasing a time step for classical trajectories should solve this problem, but increases computational time. Figure 1 also shows a reasonable agreement between the results obtained by the present method and the quantum one. This allows one to apply the proposed approach to the processes (1)–(3) in other collisions.

Thus, the branching probability current approach described above is used in the present study of nonadiabatic nuclear dynamics for computing multichannel nonadiabatic transition probabilities and inelastic cross sections. The approach is based on (i) branching of incoming and outgoing probability currents in each of the nonadiabatic regions along all possible pathways during a collision, and (ii) the novel formula [43] for the LZ parameters expressed in terms of adiabatic PECs [Eq. (23)], the parameters needed for calculations of nonadiabatic transition probabilities.

III. APPLICATION TO AL + H AND AL⁺ + H⁻ COLLISIONS

A. Simple model

The model approach described above is applied to inelastic Al + H and Al⁺ + H⁻ collisions. First, the adiabatic PECs are estimated. Since the ground ionic Al⁺ + H⁻ diabatic molecular state has the $^1\Sigma^+$ symmetry and the approach is based on nonrelativistic treatment (probabilities for transitions between states of different symmetries are negligible as compared to probabilities for transitions within the same symmetry), only molecular states of this symmetry are taken into account. In the simple version of the model the only ground ionic state and 15 lowest covalent states yielding the $^1\Sigma^+$ molecular symmetry are treated. Note that the atomic state Al($3s3p^2\,^4P$) does not provide a AlH($^1\Sigma^+$) molecular state and is not included into the present consideration, as it should have negligible cross sections for the processes treated. The atomic data are taken from [46]. The short-range parameters, $A_{ion} = 9$ a.u., $\gamma_{ion} = 1.7$ a.u., $A_{cov} = 7$ a.u., $\gamma_{cov} = 2.0$ a.u., $\tau = 2.1$ a.u., are determined by adjusting the ground adiabatic PEC to the accurate *ab initio* AlH($X^1\Sigma^+$) data [47]. The calculated 10 lowest adiabatic PECs, which have the asymptotic limits below or equal to the ionic limit, are shown in Fig. 2. Three uppermost PECs have avoided crossings with the ionic PEC at distances larger than 100 a.u., and the adiabatic splittings at these distances are so small that the system passes these nonadiabatic regions completely diabatically. For this reason only the seven lowest molecular states, six covalent and one ionic, are taken into account for the nuclear dynamical study. These states are collected in Table I. The long-range potential for the ionic channel, the state $j = 7$, is continued diabatically as ionic ($1/R$ behavior going to the ionic limit) at $R > 100$ a.u.

A series of long-range avoided crossings due to the ionic-covalent interaction is clearly seen in Fig. 2. The calculated
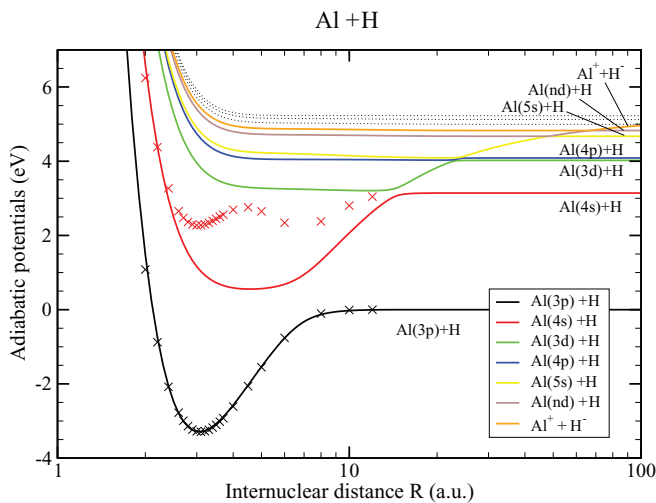
TABLE I. The AlH molecular channels, the corresponding asymptotic atomic states, and the asymptotic energies with respect to the ground state.

j	Molecular states	Asymptotic interactions	Asymptotic energies E_j^∞ (eV)[a]
1	$1^1\Sigma^+$	Al($3p^2\,P$) + H	0.0
2	$2^1\Sigma^+$	Al($4s^2\,S$) + H	3.1427
3	$3^1\Sigma^+$	Al($3d^2\,D$) + H	4.0216
4	$4^1\Sigma^+$	Al($4p^2\,P$) + H	4.0860
5	$5^1\Sigma^+$	Al($5s^2\,S$) + H	4.6729
6	$6^1\Sigma^+$	Al($nd^2\,D$) + H	4.8270
7	$8^1\Sigma^+$	Al⁺(^1S) + H⁻	5.2358

[a]NIST [46] J-weighted average values.

adiabatic splittings allow one to compute the LZ parameters by means of Eq. (23). It should be emphasized that the covalent states, Al($3d^2D$) + H and Al($4p^2P$) + H, $j = 3$ and 4, are energetically so close that the corresponding long-range nonadiabatic regions (created by interactions with the ionic state) are overlapping. It can be shown analytically, that in case of K (nearly) degenerate states interacting with another (ionic) state the present model gives a minimum of the splitting $Z_{j,j+K}$ between utmost adiabatic potentials U_j and U_{j+K}, which is equal to

$$Z_{j,j+K} = 2\sqrt{\sum_{k=1}^{K} H_{j,j+k}^2}. \tag{27}$$

It results in the following expression for the LZ parameters:

$$\xi_{j,j+K} = \sum_{k=1}^{K} \xi_{j+k-1,j+k}, \tag{28}$$

where the LZ parameter $\xi_{j,j+K}$ is evaluated by means of Eq. (23) using the adiabatic potentials U_j and U_{j+K}, while $\xi_{j+k-1,j+k}$ are the conventional LZ parameters for adjacent states. In the present case of two nearly degenerate covalent states interacting with the ionic state, the off-diagonal matrix elements and the nonadiabatic regions are determined by their asymptotic energies only [see Eqs. (11)–(14)], and, hence, the LZ parameters for adjacent states are equal and can be evaluated by $\xi_{34} = \xi_{45} = \xi_{35}/2$, where the latter is calculated by means of Eq. (23) based on the potentials U_3 and U_5.

At short distances the model PECs and splittings are underestimated and deviate from the accurate *ab initio* calculations [47]. For this reason, the LZ parameter ξ_{12} is evaluated by means of Eq. (23) based on the *ab initio* data [47]. In fact, the splitting between the two lowest PECs is so large that nonadiabatic transitions between these states have negligible probabilities, as confirmed by the dynamical calculations (see below). Some additional *ab initio* calculations have been performed by Lane [48] for the $2^1\Sigma^+$ and $3^1\Sigma^+$ states, which are in agreement with the present model PECs even providing better agreement with the model $2^1\Sigma^+$ PEC in the avoided crossing region around $R \approx 14$ a.u. than the PEC from [47]. These additional calculations provide the LZ parameter ξ_{23} close to the parameter from the model PECs. To the best of our knowledge, no *ab initio* calculations for higher-lying PECs have been performed, but splittings at larger
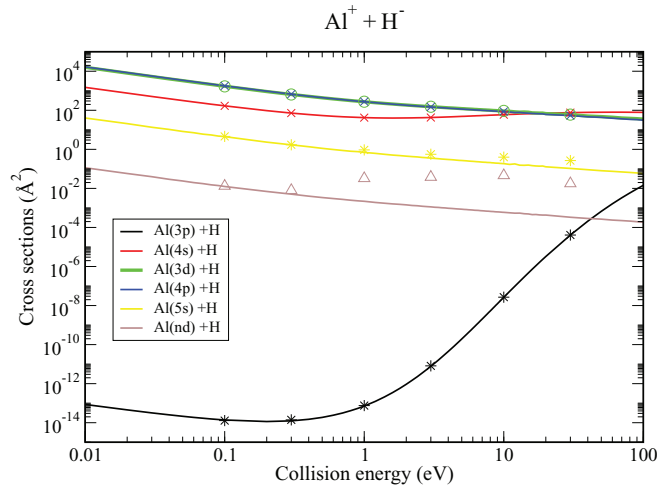

FIG. 2. (Color online) The adiabatic PECs for the lowest AlH($^1\Sigma^+$) states (lines). The solid lines plot PECs for the states which are taken into account in the dynamical treatment. The dotted lines show PECs for the states which are below the ionic limit, but their avoided crossings with the ionic PECs take place at distances larger than $R = 100$ a.u. The symbols are the accurate *ab initio* data [47].

FIG. 3. (Color online) The cross sections $\sigma_{7k}(E)$ for the mutual neutralization process in low-energy $Al^+ + H^-$ collisions (transitions from the initial state $j = 7$). The solid lines are the results of the simple model, while symbols are those of the extended model (see text). The key for the final states k is given by color and the same for all figures with the cross sections and the rates. The statistical population probabilities are included in the cross sections.

internuclear distances calculated by means of the asymptotic formulas (11)–(14) are expected to have higher accuracy than at shorter distances.

The calculated LZ parameters allow one to compute multichannel nonadiabatic transition probabilities, inelastic cross sections, and rate coefficients by means of the branching probability current method described in the previous section. As mentioned above, the branching probability current method allows one to treat both open and closed channels, as well as cases when there are several nonadiabatic regions between a pair of adjacent adiabatic PECs, the cases treated below.
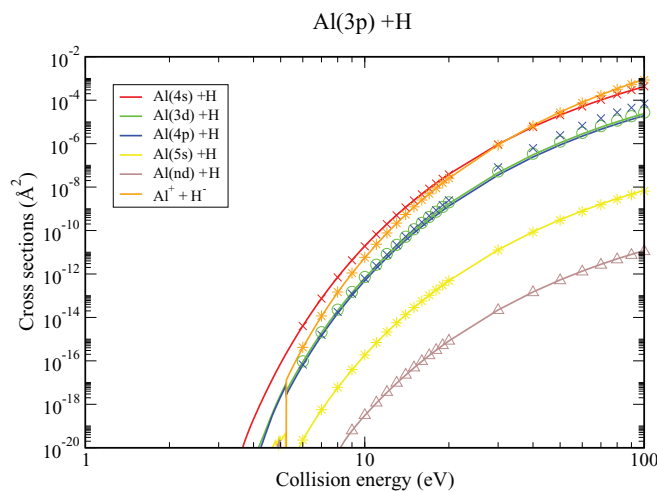
FIG. 4. (Color online) The inelastic cross sections $\sigma_{1k}(E)$ in low-energy $Al(3p) + H$ collisions (transitions from the initial state $j = 1$). The solid lines are the results of the simple model, while symbols are those of the extended model (see text). The key for the final states k is given by color and the same for all figures with the cross sections. The statistical population probabilities are included in the cross sections.
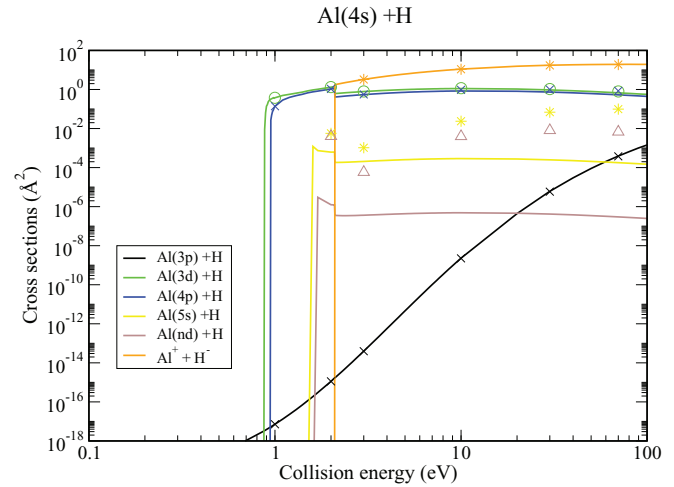

FIG. 5. (Color online) The same as in Fig. 4, but for $Al(4s) + H$ collisions, i.e., for transitions from the initial state $j = 2$.

The calculated inelastic cross sections for the processes (1)–(3) in $Al + H$ and $Al^+ + H^-$ collisions are shown in Figs. 3–9 for the collision energies from the thresholds and up to 100 eV. Each figure shows the cross sections (both upwards and downwards) for a particular initial state and all final states.

The ion-pair formation and the mutual neutralization processes (2) and (3) are typically of the main interest in astrophysical applications, as described in the Introduction. The mutual neutralization cross sections in $Al^+ + H^-$ collisions are plotted in Fig. 3, while the cross sections for the ion-pair formation in $Al(nl) + H$ collisions are shown in Figs. 4–9 (by orange lines). It is seen from this figure that the mutual neutralization leads mainly to population of the $3d$ and $4p$ states of Al. These states are energetically close to each other and have nonadiabatic regions due to ionic-covalent interaction at relatively large distances, $R \approx 23$ a.u. (see Fig. 2), with moderate splittings which result in the largest values of the cross sections [see Eq. (4)]. The next largest mutual neutralization low-energy cross section corresponds to population of the $Al(4s)$ state. The corresponding nonadiabatic region is also due to the ionic-covalent interaction and takes place at $R \approx 14$ a.u., also with a moderate splitting. The mutual neutralization cross sections for formation of the $5s$ and nd states are several orders of magnitude smaller than those for the $3d$ and $4p$ states. This fact has the clear physical explanation: The corresponding nonadiabatic regions for the $5s$ and nd states are located at large internuclear distances $R > 48$ a.u. (see Fig. 2), and this results in small adiabatic splittings, and finally small cross sections [Eq. (4)]. The nonadiabatic regions for the $5p$, $4f$, and $6s$ states, the states with the PECs plotted by dashed line in Fig. 2, are located at so large distances ($R > 100$ a.u.) that the population of these states due to ionic-covalent interactions is negligible. The formation of the ground state $3p$ has negligible low-energy cross sections due to the large adiabatic splitting, which has a minimum at around 7.8 a.u. This cross section becomes noticeable only at high collision energies, close to 100 eV.

The inelastic cross sections for the processes in $Al(nl) + H$ collisions, including the excitation and de-excitation ones, have similar features (see Figs. 4–9). Typically, the largest
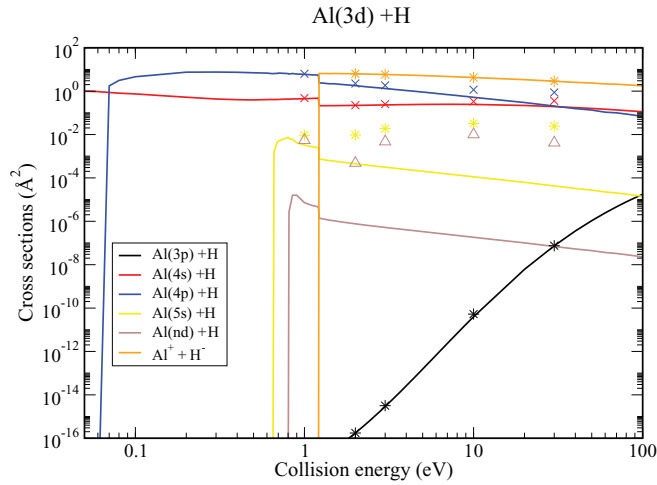
FIG. 6. (Color online) The same as in Fig. 4, but for Al(3d) + H collisions, i.e., for transitions from the initial state $j = 3$.

FIG. 8. (Color online) The same as in Fig. 4, but for Al(5s) + H collisions, i.e. for transitions from the initial state $j = 5$.

cross sections correspond to the Al$^+$ + H$^-$ formation, when the collision energy is high enough and the ionic channel is energetically open. If the ionic channel is closed, the probability currents perform oscillations between classical turning points on the left and on the right among different adiabatic PECs including the ionic one; during these oscillations a probability current decays into energetically open channels on each oscillation. In this case, the multichannel formula Eq. (15) is not valid any more, but the branching probability current method can handle these situations. For these low energies, the largest cross sections correspond mainly to transitions between the 3d and 4p states (excitation and de-excitation); the transitions involving the 4s state also have rather large cross sections. Increasing the collision energy above the energy thresholds for the ionic channel leads to steps down in energy dependence of excitation (de-excitation) cross sections. The physical background of these steps is the following. Outgoing currents in the ionic channel are typically significant. When a total energy is below the asymptotic PEC for this channel, these outgoing currents return back
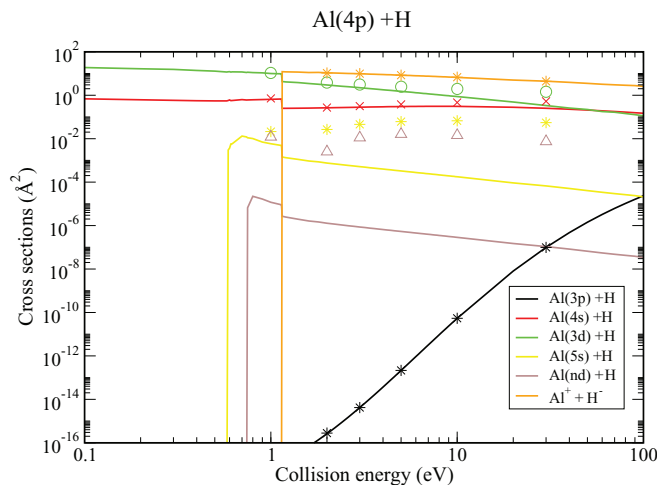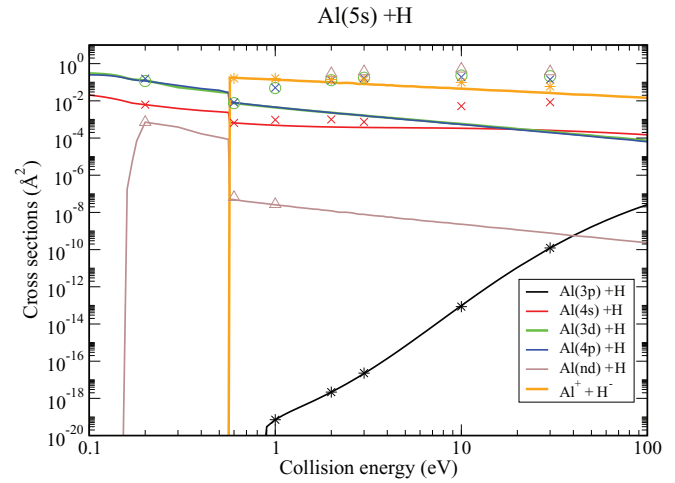
providing substantial populations (and, finally, cross sections) of open channels due to above-mentioned oscillations between classical turning points. As soon as the ionic channel gets open, these outgoing currents populate the ionic channel resulting in significant drops down of both covalent-channel populations and excitation cross sections.

It is worth noticing that the largest cross sections in Al(nl) + H collisions are of the values of 10–20 Å^2, mainly for the ion-pair formation and also for transitions (excitation and de-excitation) between the 3d and 4p states with the small energy threshold (see Figs. 6 and 7). The latter results in large rate coefficients (see below). All cross sections for collisions from the ground state Al(3p) have very small values due to large energy gap (see Fig. 4).

The rate coefficients $K_{jk}(T)$ for the excitation and the ion-pair formations processes, that is, for the upwards transitions $j \to k$, $k > j$, are plotted in Figs. 10–15 as a function of a temperature T. The rates for the inverse processes, the downwards transitions $k \to j$ (de-excitation and mutual

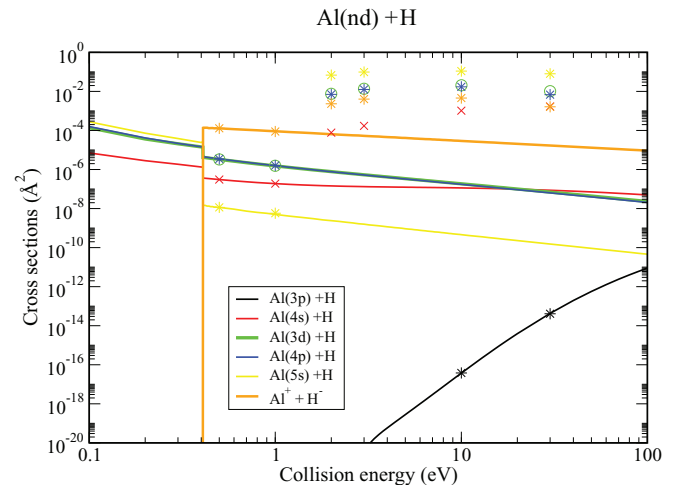FIG. 7. (Color online) The same as in Fig. 4, but for Al(4p) + H collisions, i.e., for transitions from the initial state $j = 4$.

FIG. 9. (Color online) The same as in Fig. 4, but for Al(nd) + H collisions, i.e., for transitions from the initial state $j = 6$.

Al(3p) +H
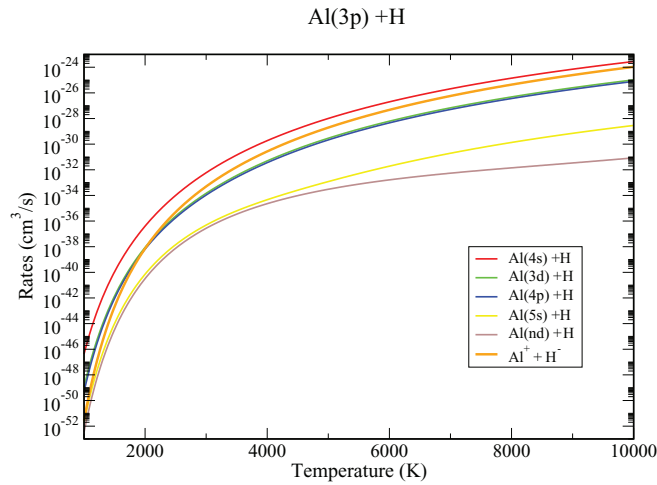
FIG. 10. (Color online) The inelastic rate coefficients $K_{1k}(T)$ for Al(3p) + H collisions, i.e., for transitions from the initial state $j = 1$, as a function of a temperature T. The key for the final states k is given by color and the same for all figures with the rates.

neutralization), can be calculated by using detailed balance,

$$K_{kj}(T) = K_{jk}(T)\, \frac{p_k^{\text{stat}}}{p_j^{\text{stat}}}\, \exp\left(\frac{\Delta E_{kj}}{k_B T}\right), \qquad (29)$$

$\Delta E_{kj} = E_k - E_j$ being the energy defect. As expected from the calculated cross sections, the largest rates (up to 10^{-9} cm^3/s) correspond to the excitation process between the two energetically close states, $3d$ and $4p$, and to the ion-pair formation process from these states (Figs. 12 and 13). The next largest rates, roughly by one-two orders of magnitude smaller (depending on a temperature), correspond to the $4s \to 3d$, $4s \to 4p$ excitation and the ion-pair formation from the $4s$ and $5s$ states (Figs. 11 and 14). Other processes have smaller rate coefficients.
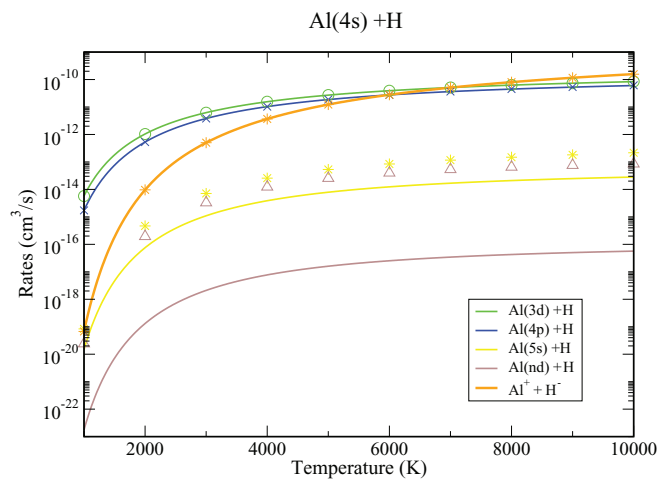

Al(4s) +H

FIG. 11. (Color online) The inelastic rate coefficients $K_{2k}(T)$ for Al(4s) + H collisions, i.e., for transitions from the initial state $j = 2$, as a function of a temperature T. The solid lines are the results of the simple model, while symbols are those of the extended model (see text). The key for the final states k is given by color and the same for all figures with the rates.
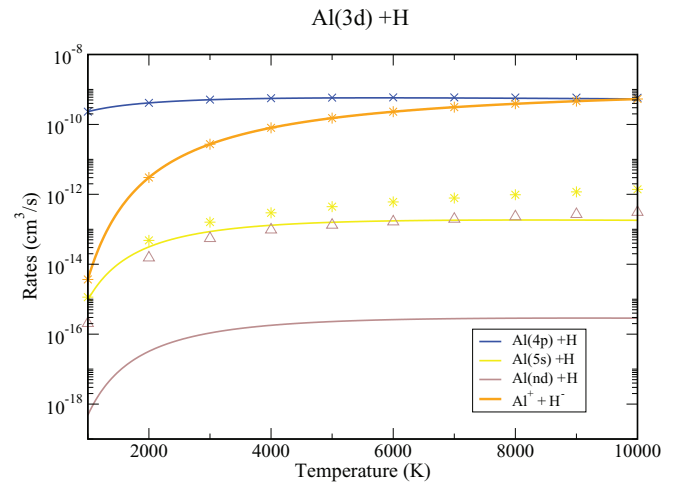
Al(3d) +H

FIG. 12. (Color online) The same as in Fig. 11, but for Al(3d) + H collisions.

For the inverse processes, the largest rates correspond to the mutual neutralization into the $3d$ and $4p$ states (both rates of the order of 5×10^{-8} cm^3/s), as well as into the $4s$ state (of the order of 6×10^{-9} cm^3/s), all due to the large upwards rates K_{jk} and the large energy defects ΔE_{kj} [see Eq. (29)]. The next largest rate is for the $4p \to 3d$ de-excitation with a value of 10^{-9} cm^3/s. The rates for the mutual neutralization process are shown in Fig. 16 (the rates into the $3p$ and $4p$ states nearly coincide within the figure scale). It is seen that the largest rates are nearly constant over a wide range of temperature.

It should be emphasized that all processes discussed in this subsection are based on the ionic-covalent interaction at large distances taken into account in the simple model. An influence of nonadiabatic regions at shorter internuclear distances is treated in the next subsection.

B. Extended model

The extension of the simple model discussed above is performed by taking into account nonadiabatic regions at short and intermediate distances. Physical evidence and analysis of
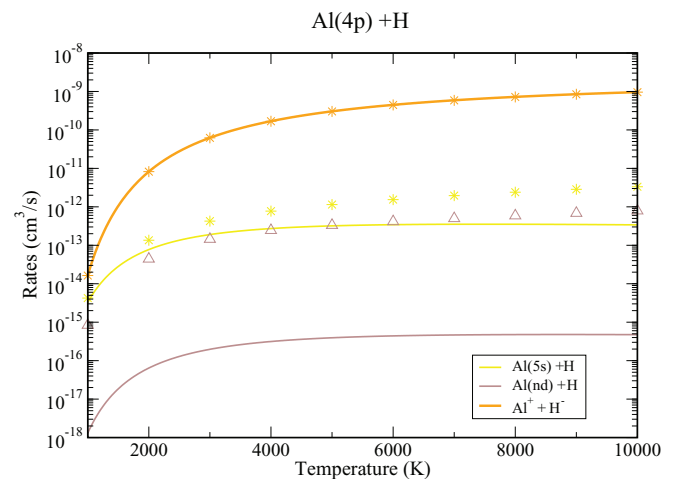
Al(4p) +H

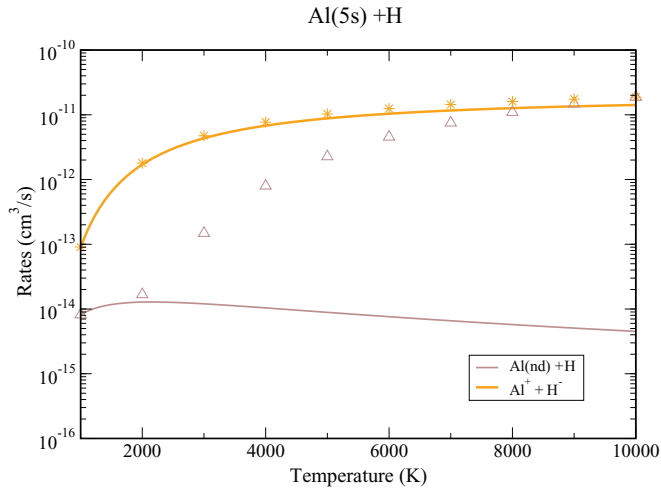FIG. 13. (Color online) The same as in Fig. 11, but for Al(4p) + H collisions.

FIG. 14. (Color online) The same as in Fig. 11, but for Al(5*s*) + H collisions.

accurate quantum-chemical data for excited molecular states of the similar systems, e.g., MgH [9,14], NaH [12], and LiH [11], show that nonadiabatic regions between excited molecular states exist not only at large, but also at intermediate and short internuclear distances. They are due to interactions between covalent states, as well as due to interactions with other ionic states asymptotically corresponding to excited positive ions. The shape of the 2 $^1\Sigma^+$ *ab initio* PEC [47] shown in Fig. 2 clearly indicates an additional avoided crossing between the 2 $^1\Sigma^+$ and the 3 $^1\Sigma^+$ adiabatic PECs around $R \approx 2.7$ a.u. The quantal treatments of nonadiabatic nuclear dynamics in inelastic Li, Na, Mg + H collisions [7,8,10] show that there are several mechanisms of inelastic processes in collisions with H; some of them correspond to nonadiabatic transitions at short and intermediate internuclear distances. In order to estimate an influence of these nonadiabatic regions on inelastic cross sections and rate coefficients, the simple model described above is extended in this subsection by increasing a number of nonadiabatic regions by several additional nonadiabatic regions between adjacent excited molecular states at distances
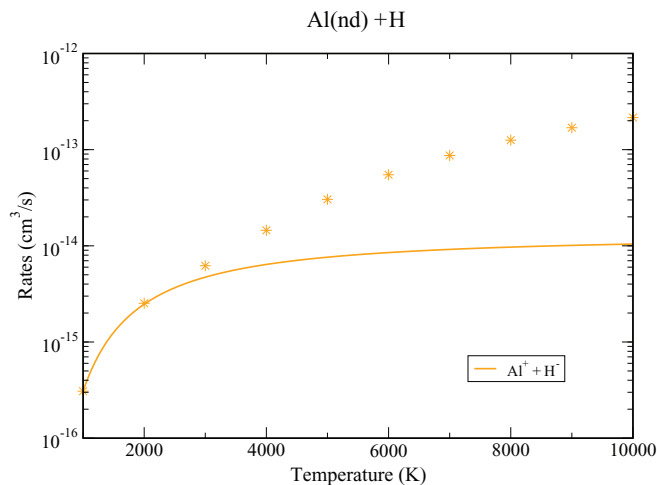

FIG. 15. (Color online) The same as in Fig. 11, but for Al(*nd*) + H collisions.

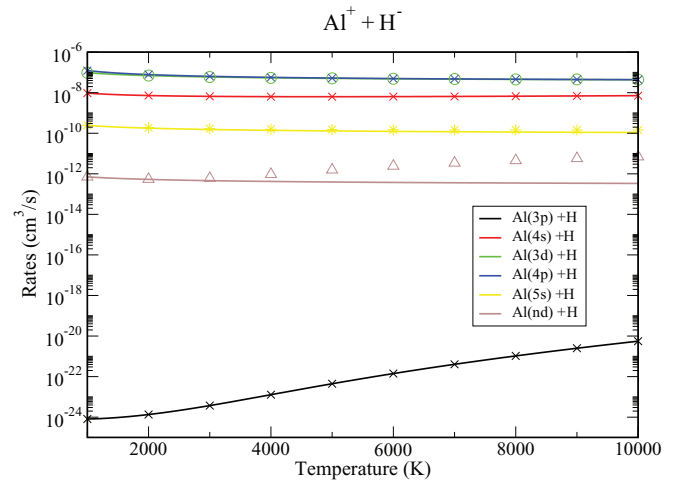
FIG. 16. (Color online) The inelastic rate coefficients for Al$^+$ + H$^-$ collisions, that is, for the mutual neutralization process. The key for the final states is the same as in Fig. 11.

$R < 10$ a.u. The additional nonadiabatic region between the 2 $^1\Sigma^+$ and the 3 $^1\Sigma^+$ states was determined from the data of Ref. [48]. The locations of other additional regions were estimated from a diabatic PEC for excited ionic state and on an analogy with MgH [9,14]. Finally, six additional nonadiabatic regions in the internuclear distance region between 2.7 and 6.0 a.u. have been added. It is worth noticing that although the additional regions are not specified explicitly by the model, their existence is justified by physical arguments. Moreover, as shown below, they give some corrections only for inelastic cross sections with moderate and small values. Thus, the inclusion of the additional nonadiabatic regions into the nuclear dynamics improves the results.

The inelastic cross sections calculated by means of the extended model are shown in Figs. 3–9 by symbols. The color of the symbols corresponds to the final states of the treated processes and is the same for the cross sections obtained by means of the simple model. It is seen that the cross sections with large values, roughly larger 1 Å^2, for the transitions between the 4*s*, 3*d*, 4*p*, and ionic states, practically are not affected by inclusion of short-range nonadiabatic regions. This is a consequence of the fact that these processes are based on nonadiabatic transitions with large probabilities in the long-range regions formed by the ionic-covalent interaction and, hence, the cross sections are mainly determined by large J [see Eq. (24)]. The long-range nonadiabatic regions are well described by the simple model, and the presence of short-range nonadiabatic regions, which may contribute in partial waves only with small J, does not change noticeably the inelastic cross sections.

The next finding of the extended model is that some cross sections, for which the simple model provides rather small values, are increased substantially by the inclusion of short-range nonadiabatic regions, up to several orders of magnitude. This takes place for transitions, for which the long-range avoided crossings with small splittings yield small probabilities $\bar{P}_{if}$ [see Eq. (4)]. In this case, transitions at short distances increase the probabilities $\bar{P}_{if}$ substantially finally increasing cross sections, but since R_{nonad} are rather small,
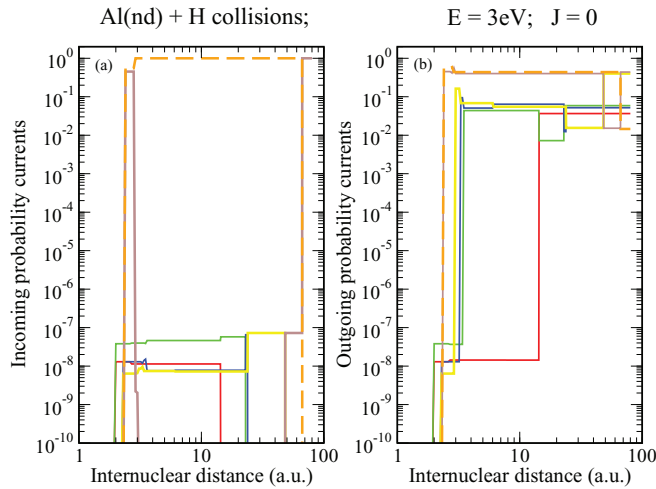
FIG. 17. (Color online) The incoming (a) and outgoing (b) probability currents in different adiabatic molecular states for Al(nl) + H collisions at $E = 3$ eV and $J = 0$ as a function of the internuclear distance. The key for the states is given by color and the same as in Fig. 2. The currents for the ionic adiabatic state are depicted by dashed (orange) lines.

the inelastic cross sections have only moderate values [see Eq. (4)]. As an example, let us consider collisions Al(nd) + H, $j = 6$. The long-range avoided crossing between the $6^1\Sigma^+$ and $7^1\Sigma^+$ states is located at $R \approx 67$ a.u. with the minimum of the adiabatic splitting of 3.4×10^{-7} a.u., providing the small value for the LZ parameter $\xi = 8.1 \times 10^{-10}$ a.u. The system passes this region nearly diabatically, and the simple model yields small inelastic cross sections for all transitions, not exceeding 10^{-4} Å^2 (see Fig. 9). The distribution of the probability current changes with the inclusion of the short-range nonadiabatic regions, that is, within the extended model. The incoming and outgoing probability currents calculated by means of the branching current method are shown in Fig. 17 for the collision energy $E = 3$ eV and $J = 0$ within the extended model. Within this model, after diabatical passing the long-range avoided crossing on the way in (the incoming current transfers practically entirely from the $6^1\Sigma^+$ into the $7^1\Sigma^+$ adiabatic state), the incoming current splits at short distances (at $R \approx 2.8$ a.u. in the present case) populating different molecular states (in the present case, the $6^1\Sigma^+$ and $7^1\Sigma^+$ states) [see Fig. 17(a)]. Note that in the case treated, the probability currents in other states (due to the long-range transitions) have small values, not exceeding 10^{-7}, while the currents due to short-range transitions have rather large values, of order of unity [see Fig. 17(a)]. On the way out, Fig. 17(b), the short-range nonadiabatic regions distribute the outgoing currents populating practically all adiabatic states with the noticeable probability currents, larger than 10^{-2}, and then the system passes the long-range avoided crossings (in different states) nearly diabatically again, providing noticeable outgoing probability currents in different channels, including ionic. Thus, the inclusion of the short-range nonadiabatic regions (the extended model) substantially increases some transition probabilities and, finally, some inelastic cross sections (see Figs. 3 and 5–9. For the ion-pair formation process (2), the extended model describes a population of the ionic channel by means

of the so-called loop mechanism, which was found in the quantum treatment (see Ref. [10]). This mechanism involves short-range transitions. Ultimately, short-range transitions for both (de-)excitation and ion-pair formation processes yield inelastic cross sections typically not exceeding 10^{-3}–1 Å^2 according to Eq. (4). It should be emphasized that although the increase of cross sections due to applying of the extended model is noticeable, the largest cross sections are still due the ionic-covalent interaction when the corresponding avoided crossings have optimal LZ parameters.

The cross sections involved the ground molecular state and calculated within the simple and the extended models practically coincide, as the ground-state PEC is energetically well separated from other PECs. These cross sections have negligibly small values, so the processes with participation of the ground atomic state Al($3p$) can be neglected in astrophysical applications. This is typical for collisions of H with other atoms, see, e.g., [7,8,10].

The increase of inelastic cross sections by inclusion of short-range nonadiabatic regions takes place at relatively high collision energies, typically higher than 1 eV (see Figs. 3–9. Since the rate coefficients of interest are at relatively low temperatures, 1000–10 000 K, the rates are determined by low collision energies, usually near energy thresholds, where deviations of the cross sections obtained by the simple and the extended models are small, so the rate coefficients calculated within the simple and the extended models are expected to differ not much. The calculated rates obtained within the simple and the extended models are compared in Figs. 10–16. The comparison shows that indeed the rates with large values are obtained with high accuracy. For transitions with moderate and small values for the rate coefficients, except for those involving Al($3p$) for which all rates coincide, the extended model provides larger rates than the simple model, especially at higher temperatures.

IV. DISCUSSION AND CONCLUSION

A model approach is derived for estimating cross sections and rate coefficients of inelastic processes (excitation, de-excitation, ion-pair formation, mutual neutralization) in low-energy collisions of hydrogen atoms and its negative ions with other atoms and their positive ions. In the present paper, the approach is applied to Al + H and Al$^+$ + H$^-$ collisions, which are of astrophysical interest. The analysis of the calculated cross sections and rates allows one to divide the processes treated into three groups.

The first group consists of the processes with large values for cross sections and rates, roughly with cross sections larger than 1 Å^2. These inelastic processes are based on nonadiabatic transitions due to the ionic-covalent interaction at large internuclear distances. For these processes a presence of additional nonadiabatic regions at short to intermediate internuclear distances (roughly, shorter than 10 a.u.) practically does not affect the cross sections obtained by means of the simple model based on long-range regions only. The parameters of these long-range nonadiabatic regions are well defined by the derived model, so the calculated estimates for the corresponding cross sections and rates are expected to be accurate within a factor of 2 or 3. The main feature of processes

in this group is that the long-range nonadiabatic parameters are optimal for transitions, and this selects covalent states (and, hence, atomic states) in the optimal window. The interaction of these optimal-window covalent states with the ionic state provides large values of cross sections and rates for excitation and de-excitation processes between these states, as well as for ion-pair formation and mutual neutralization processes between these states and the ionic state. The optimal window is typically determined by nonadiabatic regions located at internuclear distances of 15–30 a.u. For the AlH system, the optimal window selects the Al($3d$) and Al($4p$) states, so the excitation and de-excitation processes between these states, as well as the ion-pair formation and mutual neutralization processes involving these states have the largest cross sections. The state Al($4s$) is at the border of the optimal window, so the corresponding processes involving this state have relatively large cross sections as well, but smaller than the maximal ones (up to 20 Å^2 for endothermic processes). The inelastic processes involving the states from this group are expected to be important for astrophysical applications.

The second group includes processes with small to moderate cross sections and rates. Long-range nonadiabatic regions formed by the ionic-covalent interaction are beyond the optimal window, so the system traverses these regions nearly diabatically for states above the optimal window or adiabatically for states below the optimal window, any case resulting in rather small nonadiabatic transition probabilities at large internuclear distances. A presence of short-range nonadiabatic regions between covalent states increases cross sections up to several orders of magnitude, but short-range transitions can provide only moderate values for inelastic cross sections, typically not exceeding 10^{-3} to 1 Å^2, and increase is more significant at high collision energies while the main astrophysical interest is in low energies. Although short-range nonadiabatic regions are not well specified by the present model, their presence is justified by physical reasons. In addition, short-range transitions could take places between molecular states of symmetries different from the ionic one ($^1\Sigma^+$ in the present case), so this fact also verifies the inclusion of short-range nonadiabatic regions. The presence of short-range nonadiabatic regions provides substantial values for cross sections either via a direct covalent-transition mechanism for excitation and de-excitation processes involving these

states, or via the loop mechanism (see Ref. [10] and the discussion above) for the processes involving the ionic state. For the AlH system, the second group includes processes involving the Al($5s$) and Al(nd) states, as well as higher-lying states. The obtained estimates for this group are expected to be reliable within a factor of 2–10. These processes may have some effects in astrophysical applications.

The third group consists of the processes with negligible values of cross sections and rates. Low-lying states (including the ground state) are typically in this group. Adiabatic potentials for low-lying states usually have large energy gaps, so nonadiabatic transition probabilities are very small. The inclusion of additional nonadiabatic regions or additional mechanisms (see Ref. [10] for different reaction mechanisms) can increase them by several orders of magnitude, but they are still negligible.

It is worth mentioning that the limits of the optimal window are ambiguous and energy dependent; increasing a collision energy shifts the window down. For low collision energies, the optimal window limits are not so sensitive and determined mainly by collision energies near thresholds. For each atom of interest, the optimal window selects atomic states with large inelastic cross sections and rates, and this selection is determined by an atomic energy-level structure.

The derived model approach explains the results of quantum calculations for the mutual neutralization processes in low-energy collisions Li + H [11,49], Na + H [8], and Mg + H [10]: The most populated states, Li($3s$), Na($4s$), and Mg($3s4s^1S$), as well as the neighboring states with significant populations are located in the optimal window.

It should be emphasized that although the present finding is based on the results of the particular case of Al + H and Al$^+$ + H$^-$ collisions, the derived model and the conclusions are general.

ACKNOWLEDGMENTS

[1] D. L. Lambert, Phys. Scr. T **47**, 186 (1993).

[2] M. Asplund, Annu. Rev. Astron. Astrophys. **43**, 481 (2005).

[3] P. S. Barklem, Astron. Astrophys. **466**, 327 (2007).

[4] M. Bergemann, K. Lind, R. Collet, and M. Asplund, J. Phys.: Conf. Series **328**, 012002 (2011).

[5] P. S. Barklem, J. Phys.: Conf. Series **397**, 012049 (2012).

[6] A. K. Belyaev, J. Grosser, J. Hahne, and T. Menzel, Phys. Rev. A **60**, 2151 (1999).

[7] A. K. Belyaev and P. S. Barklem, Phys. Rev. A **68**, 062703 (2003).

[8] A. K. Belyaev, P. S. Barklem, A. S. Dickinson, and F. X. Gadéa, Phys. Rev. A **81**, 032706 (2010).

[9] M. Guitou, A. K. Belyaev, P. S. Barklem, A. Spielfiedel, and N. Feautrier, J. Phys. B **44**, 035202 (2011).

[10] A. K. Belyaev, P. S. Barklem, A. Spielfiedel, M. Guitou, N. Feautrier, D. S. Rodionov, and D. V. Vlasov, Phys. Rev. A **85**, 032704 (2012).

[11] H. Croft, A. S. Dickinson, and F. X. Gadéa, J. Phys. B **32**, 81 (1999).

[12] A. S. Dickinson, R. Poteau, and F. X. Gadéa, J. Phys. B **32**, 5451 (1999).

[13] A. K. Belyaev, Eur. Phys. J. D **44**, 497 (2007).

[14] M. Guitou, A. Spielfiedel, and N. Feautrier, Chem. Phys. Lett. **488**, 145 (2010).

[15] P. S. Barklem, A. K. Belyaev, and M. Asplund, Astron. Astrophys. **409**, L1 (2003).

[16] P. S. Barklem, A. K. Belyaev, A. S. Dickinson, and F. X. Gadéa, Astron. Astrophys. **519**, A20 (2010).

[17] P. S. Barklem, A. K. Belyaev, A. Spielfiedel, M. Guitou, and N. Feautrier, Astron. Astrophys. **541**, A80 (2012).

[18] K. Lind, M. Asplund, and P. S. Barklem, Astron. Astrophys. **503**, 541 (2009).

[19] K. Lind, M. Asplund, P. S. Barklem, and A. K. Belyaev, Astron. Astrophys. **528**, A103 (2011).

[20] L. Mashonkina, Astron. Astrophys. **550**, A28 (2013).

[21] W. Steenbock and H. Holweger, Astron. Astrophys. **130**, 319 (1984).

[22] H.-W. Drawin, Z. Phys. **211**, 404 (1968); **225**, 483 (1969); H.-W. Drawin and F. Emard, Phys. Lett. A **43**, 333 (1973).

[23] P. S. Barklem, A. K. Belyaev, M. Guitou, N. Feautrier, F. X. Gadéa, and A. Spielfiedel, Astron. Astrophys. **530**, A94 (2011).

[24] N. N. Shimanskaya, L. I. Mashonkina, and N. A. Sakhibullin, Astronomy Reports **44**, 530 (2000).

[25] J. O. Sundqvist, N. Ryde, G. M. Harper, A. Kruger, and M. J. Richter, Astron. Astrophys. **486**, 985 (2008).

[26] G. Zhao, K. Butler, and T. Gehren, Astron. Astrophys. **333**, 219 (1998).

[27] R. Diehl, H. Halloin, K. Kretschmer *et al.*, Nature (London) **439**, 45 (2006).

[28] S. M. Andrievsky, M. Spite, S. A. Korotin, F. Spite, P. Bonifacio, R. Cayrel, V. Hill, and P. Francois, Astron. Astrophys. **481**, 481 (2008).

[29] A. F. Marino, A. P. Milone, G. Piotto, S. Villanova, L. R. Bedin, A. Bellini, and A. Renzini, Astron. Astrophys. **505**, 1099 (2009).

[30] E. Carretta, V. D'Orazi, R. G. Gratton, and S. Lucatello, Astron. Astrophys. **543**, A117 (2012).

[31] N. F. Mott and H. S. W. Massey, *The Theory of Atomic Collisions* (Clarendon, Oxford, 1949).

[32] A. Macías and A. Riera, Phys. Rep. **90**, 299 (1982).

[33] L. D. Landau, Phys. Z. Sowietunion **1**, 88 (1932); **2**, 46 (1932); C. Zener, Proc. Roy. Soc. A **137**, 696 (1932).

[34] P. J. Bruna and S. D. Peryerimhoff, Adv. Chem. Phys. **67**, 1 (1987).

[35] W. C. Stwalley, W. T. Zemke, and S. C. Yang, J. Phys. Chem. Ref. Data **20**, 153 (1991).

[36] A. K. Belyaev and J. Grosser, J. Phys. B **29**, 5843 (1996).

[37] R. E. Olson, F. T. Smith, and E. Bauer, Appl. Optics **10**, 1848 (1971).

[38] C. Herring, Rev. Mod. Phys. **34**, 631 (1962).

[39] Yu. N. Demkov and V. I. Osherov, Sov. Phys. JETP **26**, 916 (1967).

[40] A. Salop and R. E. Olson, Phys. Rev. A **13**, 1312 (1976).

[41] A. K. Belyaev and S. I. Tserkovnyi, Opt. Spektrosk. **63**, 968 (1987) [Opt. Spectrosc. (USSR) **63**, 569 (1987)].

[42] A. K. Belyaev, Phys. Rev. A **48**, 4299 (1993).

[43] A. K. Belyaev and O. V. Lebedev, Phys. Rev. A **84**, 014701 (2011).

[44] J. C. Tully, J. Chem. Phys. **93**, 1061 (1990).

[45] C. F. Kammerer and C. Lasser, J. Chem. Phys. **128**, 144102 (2008).

[46] A. Kramida, Yu. Ralchenko, and J. Reader (and NIST ASD Team) NIST Atomic Spectra Database, Version 5.0 [http://physics.nist.gov/asd] (National Institute of Standards and Technology, Gaithersburg, 2012).

[47] N. Wells and I. C. Lane, Phys. Chem. Chem. Phys. **13**, 19018 (2011).

[48] I. C. Lane (private communication).

[49] H. Croft, A. S. Dickinson, and F. X. Gadéa, MNRAS **304**, 327 (1999).